


Article

Liquid-Phase Non-Thermal Plasma Discharge for Fuel Oil Processing

Evgeniy Yurevich Titov *, Ivan Vasilevich Bodrikov, Anton Igorevich Serov, Yuriy Alekseevich Kurskii, Dmitry Yurievich Titov and Evgenia Ruslanovna Bodrikova

Technology of Electrochemical Production and Chemistry of Organic Substances, Nizhny Novgorod State Technical University n.a. R.E. Alekseev, 603950 Nizhny Novgorod, Russia; orgchim@nntu.ru (I.V.B.); anton.serov710@gmail.com (A.I.S.); kurskv@yandex.ru (Y.A.K.); d.titov@nntu.ru (D.Y.T.); bodrikovaer@mail.ru (E.R.B.)

* Correspondence: e.titov@nntu.ru; Tel.: +7-950-609-96-73

Abstract: The non-thermal plasma pyrolysis of fuel oil, under the action of low-voltage electric discharges in the liquid phase, has made it possible to develop a new process to obtain valuable petrochemical products. In this study, the main parameters, including pulse energy and the time of impact on the non-thermal plasma pyrolysis process, are studied. The main components of the obtained gaseous products are hydrogen (27.6–49.6 mol%), acetylene (33.6–49.1 mol%), ethylene (6.9–12.1 mol%), methane (3.9–9.1 mol%), and hydrocarbons C3–C5 (3.8–9.3 mol%). Increasing the capacity of electric discharges leads to an increase in the content of acetylene in the gas phase to 49.1 mol% and a decrease in energy costs for the production of gaseous products.

Keywords: plasma pyrolysis; pulse electric discharge; non-equilibrium low-temperature plasma; fuel oil; hydrogen power; acetylene; ethylene



Citation: Titov, E.Y.; Bodrikov, I.V.; Serov, A.I.; Kurskii, Y.A.; Titov, D.Y.; Bodrikova, E.R. Liquid-Phase Non-Thermal Plasma Discharge for Fuel Oil Processing. *Energies* **2022**, *15*, 3400. <https://doi.org/10.3390/en15093400>

Academic Editor: Keiichiro Yoshida

Received: 21 April 2022

Accepted: 5 May 2022

Published: 6 May 2022

Publisher's Note: MDPI stays neutral with regard to jurisdictional claims in published maps and institutional affiliations.



Copyright: © 2022 by the authors. Licensee MDPI, Basel, Switzerland. This article is an open access article distributed under the terms and conditions of the Creative Commons Attribution (CC BY) license (<https://creativecommons.org/licenses/by/4.0/>).

1. Introduction

Across the world, heavy oil reserves are estimated [1] to be 5.5 trillion barrels and significantly higher than conventional oil reserves. Heavy oils are characterized by a high viscosity and density; a low ratio of hydrogen to carbon; and a high content of heterocompounds, asphaltenes, and metals. The development of new technologies for the processing of heavy oil into transport fuel and petrochemical raw materials [2,3] is an important task to fill the impending energy deficit of light hydrocarbon raw materials in the industry [4–6]. Traditional commercially available technologies for carbon removal and hydrogen addition are partially applicable to heavy oil refining, but they have significant limitations for extra-heavy oils due to low profitability [7–9]. Thus, there is a need to explore and develop new alternatives to heavy oil refining that can be used efficiently in an industrially and environmentally sound manner.

Plasma technologies for the processing of heavy oils reduce the use of hydrogen, as well as exclude the use of expensive catalysts necessary for traditional hydrotreatment. Plasma can be divided into thermal and non-thermal plasma (NTP) [10]. The power consumption required to create a thermal plasma is relatively high (tens of kilowatts). The temperature of thermal plasma is usually higher than 10,000 °C. Consequently, it is commonly used for the production of hydrogen and gaseous hydrocarbons, such as ethylene, acetylene, and syngas [11,12]. Part of the input power for the generation of thermal plasma is lost to the increase in the temperature of the reaction system. Although high temperatures are required for thermal plasma reactions, a high power consumption to heat the system above the activation temperatures of the reactions is not economically feasible. In contrast, the input power required to generate non-thermal plasma is relatively small and does not cause a clear rise in the temperature of the reaction system.

NTP generates high-energy electromagnetic fields, energetic electrons, free radicals, excited states, and other active particles [13–15]. NTP-based hydrocarbon processing technologies can operate at or slightly above ambient temperatures [16–19]. These properties of non-thermal plasma provide great potential for technologies to degrade long-chain molecules and recombine radicals to produce light hydrocarbons. Compared to traditional hydroprocessing methods, NTP-based technologies provide advantages in terms of energy consumption, the volume of hydrogen, catalysts, and high efficiency in refining heavy crude oil into marketable products.

The use of plasma chemical pyrolysis for the conversion of liquid hydrocarbons potentially provides the possibility of creating small-sized reactors with high productivity and selectivity of the target processes in contrast to plasma formed in a gaseous medium.

Plasma process technologies have been developed by many researchers as promising methods to convert various types of hydrocarbons in order to produce hydrogen, fuel fractions, ethylene, acetylene, syngas, and other products [20–24]. Direct liquid-phase discharges provide molecule activation [25,26] since plasma is generated directly in the liquid. Such an effect leads to the formation of short-lived radicals, which stimulate secondary processes of recombination, destruction, and condensation [27–32].

In [33–36], the influences of power supply parameters on the transition of discharge modes, characteristics, and main factors affecting the formation of streamers were studied. The electrical discharge characteristics affect NTP parameters and, therefore, the composition of processed products.

This work is devoted to the study of the NTP pyrolysis of fuel oil under the action of low-voltage electric discharges in the liquid phase. Electric discharges are generated when using a 60 V DC source and various capacitances of the capacitor (1–41 mF). The main purpose of this study is to identify the optimal process conditions while varying the influence of the input power and the time of impact on the composition and yield of NTP pyrolysis products. Defining the main characteristics of the process will deepen the understanding of the NTP pyrolysis of heavy petroleum products.

2. Materials and Methods

As the object of the study, fuel oil with the following characteristics was used: density at 20 °C—0.955 g/cm³, kinematic viscosity at 100 °C—31.169 mm²/s, sulfur content—2.675%, boiling point—298.5 °C, boiling point—671.3 °C, and non-volatile residue—30.6%.

Figure 1 shows the setup of the working reactor (made of Teflon, 40 cm³ capacity) used in this study, where graphite electrodes (6 mm diameter) were mounted inside it. A DC voltage source (EA-PSI 9750-06 2U) with a constant voltage of 60 V and a variable capacity condenser of 1–41 mF was used to generate low-voltage discharges by varying the distance between the electrodes. A detailed description of the discharge control unit and impact energy calculations can be found elsewhere [18,37]. The temperature in the reactor was 80–120 °C. The resulting gas was cooled and trapped in a gas trap. The reactor was set up such that the pressure was almost constant.

The voltage and current values from VS and CS were also measured using a Rigol DS1054Z oscilloscope. The measured values of the current and voltage were processed in the MatLab program to obtain graphic images of transients over time and to determine the parameters of current pulses. The program calculates the number of pulses at each measurement interval, the duration of each pulse, and the total time of the impact of discharges on the substance, and it writes the amplitude of each pulse (the maximum value of the pulse current) to the array. Then, the average values were calculated:

- the average pulse duration

$$t_{\text{aver}} = t_{\Sigma} / n, \quad (1)$$

where t_{Σ} is the total duration of the pulses; n is the number of pulses;

- the average pulse frequency

$$f_{\text{aver}} = n/t_{\text{rec}}, \quad (2)$$

where t_{rec} is the recording time of the oscillogram;

- the average amplitude of the pulses

$$A_{\text{aver}} = A_{\Sigma}/n, \quad (3)$$

where A_{Σ} is the sum of the amplitudes of each pulse;

- the pulse energy

$$E = U_d \cdot I_d \cdot T_{\text{imp}}, \quad (4)$$

where U_d is the root mean square voltage at the time interval of the discharge; I_d is the root mean square of the current at the time interval of the discharge; and T_{ipm} is the pulse time. The average pulse energy is defined as the sum of the pulse energies divided by the number of pulses. The parameters and standard errors of electrical discharges are given in Table 1.

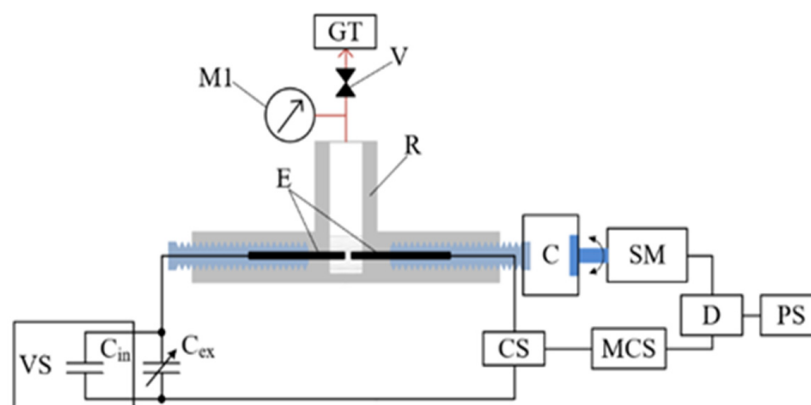


Figure 1. Scheme of the experimental setup: R—reactor; RC—reflux condenser; E—electrodes; M—manometer; V—valve; GT—gas trap; C—clutch; SM—stepper motor; D—stepper motor driver; PS—stepper motor power supply; CS—current sensor; MCS—microprocessor control system; VS—voltage source with an internal 1 mF capacitor C_{in} ; C_{ex} —external variable capacitor.

Table 1. Dependence of the characteristics of electrical discharges on the capacitance of the capacitor.

Capacitance of Capacitor, mF	1	11	21	31	41
Average pulse duration, ms	1.02 ± 0.07	8.38 ± 0.22	13.81 ± 0.33	21.24 ± 0.38	25.94 ± 0.46
Average pulse frequency, Hz	0.92 ± 0.12	0.85 ± 0.18	0.80 ± 0.22	0.76 ± 0.22	0.71 ± 0.19
Average pulse amplitude, A	71.3 ± 0.8	120.6 ± 0.6	125.3 ± 0.7	128.6 ± 1.4	136.9 ± 1.6
Average pulse energy, J	0.018 ± 0.003	0.65 ± 0.06	1.38 ± 0.08	2.59 ± 0.10	3.62 ± 0.12

The sample current and voltage for the conversion of fuel oil are shown in Figure 2. At the moment of discharge, plasma forms filamentous channels in the liquid form, which lead to inhomogeneous reactions in the liquid. After that, the electric discharge stops, and the gas bubble in the gap between the electrodes collapses.

The composition of the gas-phase products was determined by utilizing gas chromatography with flame ionization detection using a Kristall 5000.2 gas chromatograph.

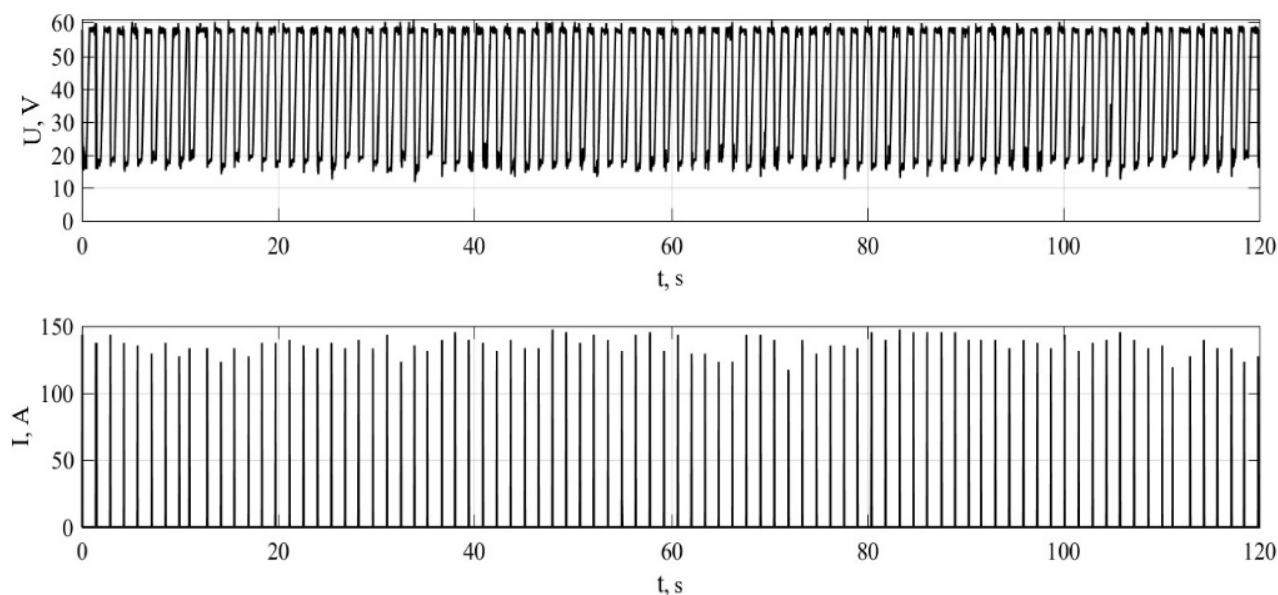


Figure 2. Oscillogram of pulses at a voltage of 60 V and capacitance of capacitor of 41 mF.

For fuel oil and liquid pyrolysis products, the following characteristics were determined: kinematic viscosity at 100 °C according to the American Society for Testing and Materials (ASTM) D7042; density at 20 °C according to ASTM D4052 using a viscometer-density meter SVM 3000, Anton Paar GmbH; sulfur content according to ASTM 4294 using an X-ray fluorescence analyzer Lab-X 3500; and fractional composition according to ASTM D7169 using a gas chromatograph Chromatek-Crystal 5000.2 with a flame ionization detector. For the infrared (IR) study of liquid products (IR Fourier spectrometer FSM 1202), liquid products were deposited on KBr windows, and the spectra of the obtained films were recorded.

The ^1H nuclear magnetic resonance (NMR) spectra were determined using a Bruker Avance III spectrometer operating at a resonance frequency of 400 MHz, accumulating 32 scans. A flip angle of 30° was set, and the delay time was set at 10 s. The signal of residual CHCl_3 ($\delta_{\text{H}} = 7.26$ ppm) in the predominantly chloroform-d solvent was used as an internal reference in these solvents. Fuel oil samples were dissolved in CDCl_3 solutions, in accordance with the ASTM D5292 method. The concentration of solutions was 5% *v/v*. Solid particles were removed by filtration. The aromaticity factors of hydrogen were obtained with the following equation [38]: $F_{\text{HA}} = H_{\text{ar}} / (H_{\text{ar}} + H_{\text{al}})$, where H_{ar} is the total integral of aromatic hydrogen, and H_{al} is the total integral of aliphatic hydrogen. The integrals of the aromatic hydrogen band were corrected by subtracting the signal of residual chloroform.

3. Results and Discussion

Areas of non-thermal plasma are formed when generating electrical discharges between electrodes. In this reaction system, active particles (secondary electrons, ions, photons, free radicals, etc.) are produced by electron–molecule collisions, and they can recombine and form lighter hydrocarbons and hydrogen [39].

Table 2 shows the experimental results regarding the effect of electric discharge with various capacitances of the capacitor (1–41 mF) and various process times (1–12 h) on the NTP pyrolysis process of fuel oil. The gaseous products mainly contain hydrogen (27.6–49.6 mol%), acetylene (33.6–49.1 mol%), ethylene (6.9–12.1 mol%), methane (3.9–9.1 mol%), and C3–C5 hydrocarbons (3.8–9.3 mol%). There is an increase in the rate of the formation of gaseous products from 0.29 to 2.2 wt% with an increase in the capacitance of the capacitor. At the same time, the content of hydrogen decreases sharply from 49.6 to 27.6 mol%, and the content of acetylene increases almost proportionally from

33.6 to 49.1 mol% in the gas phase. Other hydrocarbons, such as methane, ethylene, propane, butane, and pentane, also increase slightly.

Table 2. Characteristics of NTP pyrolysis of fuel oil and composition of gaseous products.

Condenser Capacity, mF	1	11	21	31		41		
Experiment time, h			1			1	6	12
Energy consumption, kWh	0.04	0.05	0.07	0.08	0.09	0.55	1.08	
Energy consumption, kWh/kg of gas	668	556	437	308	152	348	493	
Gas flow, ml/h	84	108	138	156	234	112	74	
		Gas yield, wt%						
Gas composition, mol%	0.29	0.375	0.6	0.95	2.2	5.94	8.36	
	H ₂	49.6	44.5	40.1	32.1	27.6	30.2	31.4
	CH ₄	3.9	5.8	6.4	7.9	7.5	7.9	9.1
	C ₂ H ₄	6.9	8.1	8.4	10.2	9.9	11.6	12.1
	C ₂ H ₆	0.3	0.5	0.6	0.7	0.8	0.8	1.0
	C ₂ H ₂	33.6	36.6	41.1	43.5	49.1	41.2	37.2
	C ₃ H ₈	0.7	1.3	1.4	2.2	2.1	3.3	3.7
	C ₃ H ₄	3.1	2.3	1.2	1.8	1.4	1.4	1.3
	1,3-C ₄ H ₆	0.1	0.1	0.1	0.3	0.2	0.7	0.8
	n-C ₄ H ₁₀	0.1	0.1	0.1	0.2	0.3	0.6	0.6
	neo-C ₅ H ₁₂	0.2	0.2	0.4	0.7	0.8	1.8	1.9

The fuel oil residue in the reactor becomes heavier (Table 3 and Figure 3) with an increase in the degree of fuel oil conversion and in the NTP pyrolysis time. The distillation curves of the initial fuel oil and the NTP pyrolysis product show that the pyrolysis process results in an increase in the boiling point of the products and a decrease in the proportion of volatile components from 69.4 to 47.6%.

There is an increase in density from 0.955 to 0.971 g/cm³ and kinematic viscosity from 31.169 to 95.699 mm²/s when the NTP pyrolysis time increases to 12 h. This is in good agreement with the data on the composition of the obtained gaseous products (Table 2). The hydrogen content increases from 27.6 to 31.4 mol% and the acetylene content decreases from 49.1 to 37.2 mol% with the increase in fuel oil conversion.

In the ¹H NMR spectra, the signals in the regions of 7.24–6.5, 8.3–7.3, and 9.0–8.3 ppm (Table 4) belong to the monoaromatic CH bond, diaromatic CH, and tri (and more) aromatic CH, respectively [40,41]. Aromatic hydrocarbons with one ring (δ_{H} 7.24–6.5 ppm) first begin to be exposed with an increase in the electric discharge energy. Their share in the total number of aromatic protons decreases from 53 to 43%. This increases the proportion of protons belonging to diaromatic and triaromatic CH. The proportion of aromatic hydrocarbons with three or more rings notably increases. Their share increases from 3.8 to 6.1%.

Table 3. Characteristics of fuel oil and NTP products—fuel oil pyrolysis at a voltage of 60 V and capacitance of capacitor of 41 mF.

	Fuel Oil	NTP Pyrolysis Products		
		1	6	12
Experiment time, h				
Density at 20 °C, g/cm ³	0.955	0.957	0.963	0.971
Kinematic viscosity at 100 °C, mm ² /s	31.169	33.705	40.927	95.699
Sulfur content, %	2.675	2.680	2.710	2.765
Non-volatile residue, %	30.6	45.5	48.1	52.4
Initial boiling point, °C	298.5	274.5	291.4	289.3
Final boiling point, °C	671.3	671.7	711.3	721.6
Volume of stripping, %	69.4	54.5	51.9	47.6

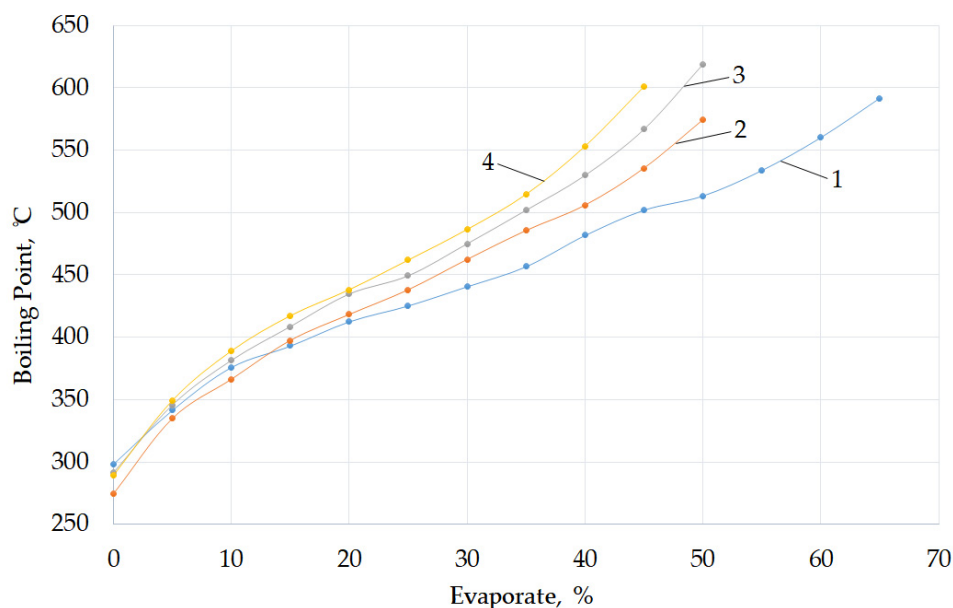


Figure 3. Fractional composition of fuel oil (1) and NTP products—fuel oil pyrolysis at experimental times of 1 h (2), 6 h (3), 12 h (4).

Table 4. ^1H NMR analysis of fuel oil and NTP pyrolysis products.

NMR ^1H Range, ppm		9.0–8.3	8.3–7.3	7.24–6.5	4.4–2.4	2.4–2.1	2.1–1.05	1.05–0.3	F_{HA}
Capacity, mF	Experiment Time, h	H_{ar} , %			H_{alr} , %				
	Fuel oil	0.19	2.26	2.55	7.85	2.78	62.83	21.55	0.0499
1	1	0.22	2.38	2.51	7.89	3.10	62.35	21.55	0.0511
11	1	0.28	2.72	2.00	8.75	2.85	61.99	21.40	0.0500
21	1	0.30	2.62	2.18	8.56	2.88	62.29	21.15	0.0511
31	1	0.30	2.77	2.00	8.45	2.91	62.23	21.34	0.0507
41	1	0.31	2.60	2.17	8.32	2.72	62.39	21.49	0.0508
41	6	0.34	2.90	2.04	8.22	2.92	61.88	21.70	0.0528
41	12	0.20	2.73	2.50	7.45	2.79	62.25	20.07	0.0543

The results of the FTIR analysis (Figure 4) are in good agreement with those of the ^1H NMR analysis. An increase in the content of aromatic (1380 cm^{-1}) and polyaromatic hydrocarbons (737 cm^{-1}) is observed in the IR spectra. It is likely that this is due to the development of the dealkylation process of aromatic compounds [42,43]. In the range of $2850\text{--}3970\text{ cm}^{-1}$, there are practically no changes in the ratio of $-\text{CH}_3$ and $-\text{CH}_2-$ groups in aliphatic hydrocarbons (Figure 4b). An interesting feature of the process is the increase observed in the IR spectrum (Figure 4a) in the proportion of CH_3 groups at the initial stage with a low exposure energy (1 mF, 1 h). According to the ^1H NMR data, these CH_3 groups appear to be attached to aromatic fragments, as the relative signal intensity increases in the region of 2.4–2.1 ppm.

These results show that, under the action of low-voltage discharges, both aliphatic and aromatic hydrocarbons are involved as indicated in the NMR analysis. In the initial reaction period, an increase in the capacitance of the capacitor (hence an increase in discharge energy) slightly increases the ratio of the aromatic protons compared to the aliphatic protons (F_{HA}) from 0.0499 to 0.0508 (Table 4). With an increase in fuel oil conversion (exposure time from 1 to 12 h), there is a significant increase in the proportion of protons in H_{ar} aromatics compared to aliphatic H_{al} ; F_{HA} increases from 0.0508 to 0.0543. This fact indicates that, in the later stages, the process of alkyl hydrocarbon decomposition is intensified together with the ring condensation process. At the same time, there is a significant decrease in the proportion

of volatile components and an increase in the boiling point (Figure 3), which is also due to the formation of condensed aromatic rings (asphaltenes) during the NTP pyrolysis of fuel oil. It is likely that the heavier fuel oil is associated with the carbonization process. The consecutive scheme [44] consists of a series of consecutive consolidation monomers and consolidation intermediates formed in condensation, polymerization, dehydrocyclization, the binding of aromatic rings, and hydrogen depletion processes until the formation of the graphite structure. In the later stages of the process, the proportion of aromatic hydrocarbons with three or more rings in the total number of aromatic protons begins to decrease from 6.1 to 3.7%.

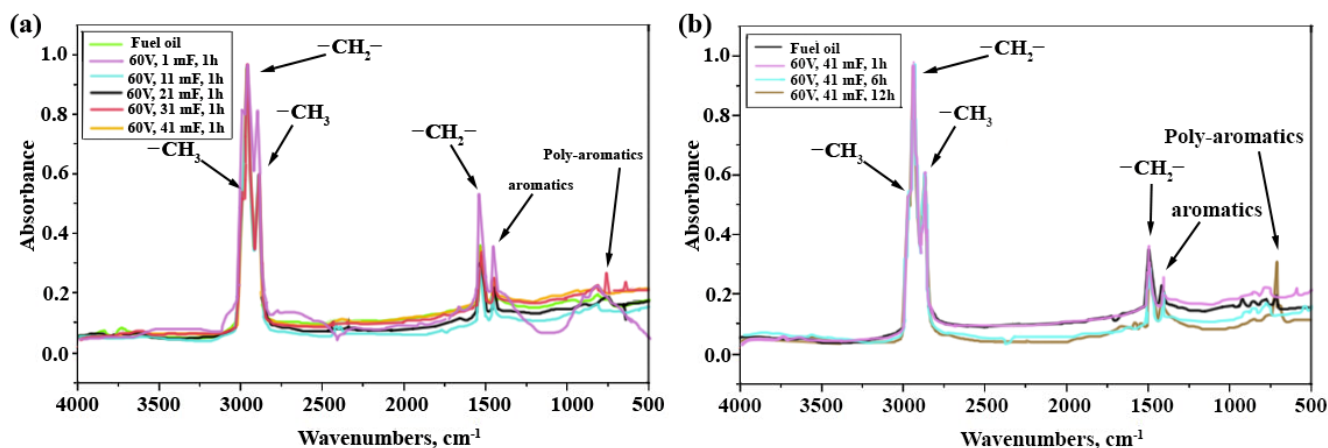


Figure 4. IR spectra of fuel oil and NTP pyrolysis product: (a) effect of capacitance of capacitor, (b) time of NTP pyrolysis process.

The energy consumption for the formation of gaseous products decreases significantly from 668 to 152 kWh/kg (Table 2), and productivity gas flow increases from 84 to 234 mL/min when there is an increase in the energy of the electric discharge. This is caused by specific energy density increases and the number of radical and active particles when exposed to an electric discharge [45,46]. A similar effect is manifested when microwave plasma is exposed to fuel oil [47]. The content of condensed aromatic hydrocarbons increases when there is an increase in the pyrolysis time of fuel oil. The excitation of condensed aromatic hydrocarbons and their splitting require more energy and lead to the higher yield of hydrogen atoms [35,48–50]; therefore, the energy costs to obtain gas in the later stages of the NTP pyrolysis process increase (Table 2).

4. Conclusions

The NTP pyrolysis of fuel oil in the liquid phase leads to the formation of gaseous products with a high content of hydrogen (27.6–49.6 mol%), acetylene (33.6–49.1 mol%), ethylene (6.9–12.1 mol%), methane (3.9–9.1 mol%), and other valuable hydrocarbons (C3–C5).

The performance, energy efficiency of the process, and the composition of the gaseous products of the NTP pyrolysis of fuel oil are significantly influenced by the energy of electric discharges and processing time. Increasing the capacitance of the capacitor of electric discharges from 1 to 41 mF provides an increase in productivity gas flow from 84 to 234 mL/min and a decrease in energy consumption for gaseous products from 668 to 152 kWh/kg of gas, as well as an increase in the concentration of acetylene from 33.6 to 49.1 mol% in the gas phase. With an increase in the time of the NTP pyrolysis process from 1 to 12 h, the energy consumption for gas formation increases from 152 to 493 kWh/kg of gas, and the hydrogen content in gas products increases from 27.6 to 31.4 mol% due to the rise in the content of condensed aromatic hydrocarbons.

Thus, the results presented in this paper show that the NTP pyrolysis of fuel oil in the liquid phase has a high potential to increase the processing depth of heavy oil fractions in order to obtain marketable and high-demand products.

Author Contributions: Conceptualization and writing—review and editing, E.Y.T.; methodology, I.V.B.; discharge control and generation system, D.Y.T.; writing—original draft preparation, A.I.S., Y.A.K., D.Y.T. and E.R.B.; experimental work, A.I.S., Y.A.K., D.Y.T. and E.R.B.; NMR analysis, Y.A.K.; analysis of petroleum products, A.I.S. and E.R.B. All authors have read and agreed to the published version of the manuscript.

Funding: This research was funded by the Russian Science Foundation, grant number 21-73-10119. <https://rscf.ru/project/21-73-10119/> (accessed on 4 May 2022).

Institutional Review Board Statement: Not applicable.

Informed Consent Statement: Not applicable.

Data Availability Statement: Not applicable.

Conflicts of Interest: The authors declare no conflict of interest.

References

1. Ganapathi, R.; Henni, A.; Shirif, E. Solubility of carbon dioxide and ethane in Lloydminster heavy oil: Experimental study and modelling. *Can. J. Chem. Eng.* **2022**, *1*. [[CrossRef](#)]
2. Shi, Q.; Zhao, S.; Zhou, Y.; Gao, J.; Xu, C. Development of heavy oil upgrading technologies in China. *Rev. Chem. Eng.* **2019**, *36*, 1–19. [[CrossRef](#)]
3. Ahmadi, M.; Chen, Z. Challenges and future of chemical assisted heavy oil recovery processes. *Adv. Colloid Interface Sci.* **2020**, *275*, 102081. [[CrossRef](#)] [[PubMed](#)]
4. Castañeda, L.C.; Muñoz, J.A.D.; Ancheyta, J. Current situation of emerging technologies for upgrading of heavy oils. *Catal. Today* **2014**, *220–222*, 248–273. [[CrossRef](#)]
5. Frączak, J.; Sharkov, N.; De Paz Carmona, H.; Tišler, Z.; Hidalgo-Herrador, J.M. Cleaner Fuel Production via Co-Processing of Vacuum Gas Oil with Rapeseed Oil Using a Novel NiW/Acid-Modified Phonolite Catalyst. *Energies* **2021**, *14*, 8497. [[CrossRef](#)]
6. Ouyang, Z.Y.; Qin, Z.; Cao, H.; Xie, T.Y.; Dai, X.Y.; Wang, Q.W. A spillover network analysis of the global crude oil market: Evidence from the post-financial crisis era. *Pet. Sci.* **2021**, *18*, 1256–1269. [[CrossRef](#)]
7. Muñoz, J.A.D.; Ancheyta, J.; Castañeda, L.C. Selection of heavy oil upgrading technologies by proper estimation of petroleum prices. *Pet. Sci. Technol.* **2022**, *40*, 217–236. [[CrossRef](#)]
8. Gulyaeva, L.A.; Khavkin, V.A.; Shmel'kova, O.I.; Vinogradova, N.Y. Technology of synthetic oil production from heavy oil stock and solid fuels. *Chem. Technol. Fuels Oils* **2015**, *51*, 422–429. [[CrossRef](#)]
9. Tan, J.; Ji, Y.N.; Deng, W.S.; Su, Y.F. Process intensification in gas/liquid/solid reaction in trickle bed reactors: A review. *Pet. Sci.* **2021**, *18*, 1203–1218. [[CrossRef](#)]
10. Bruggeman, P.J.; Kushner, M.J.; Locke, B.R.; Gardeniers, J.G.E.; Graham, W.G.; Graves, D.B.; Hofman-Caris, R.C.H.M.; Maric, D.; Reid, J.P.; Ceriani, E.; et al. Plasma-liquid interactions: A review and roadmap. *Plasma Sources Sci. Technol.* **2016**, *25*, 053002. [[CrossRef](#)]
11. Huang, W.; Jin, J.; Wen, G.; Yang, Q.; Su, B.; Ren, Q. Effect of Nitrogen/Oxygen Substances on the Pyrolysis of Alkane-Rich Gases to Acetylene by Thermal Plasma. *Energies* **2018**, *11*, 351. [[CrossRef](#)]
12. Ma, J.; Zhang, M.; Wu, J.; Yang, Q.; Wen, G.; Su, B.; Ren, Q. Hydrolysis of *n*-Hexane and Toluene to Acetylene in Rotating-Arc Plasma. *Energies* **2017**, *10*, 899. [[CrossRef](#)]
13. Bruggeman, P.; Leys, C. Non-thermal plasmas in and in contact with liquids. *J. Phys. D Appl. Phys.* **2009**, *42*, 053001. [[CrossRef](#)]
14. Lebedev, Y.A. Microwave discharges in liquid dielectrics. *Plasma Phys. Rep.* **2017**, *43*, 685–695. [[CrossRef](#)]
15. Kuzenov, V.V.; Ryzhkov, S.V. Numerical Simulation of Pulsed Jets of a High-Current Pulsed Surface Discharge. *Comput. Therm. Sci.* **2021**, *13*, 45–56. [[CrossRef](#)]
16. Bodrikov, I.V.; Ivanova, A.G.; Vasiliev, A.L.; Titov, E.Y.; Titov, D.Y.; Serov, A.I. Influence of low-voltage discharge energy on the morphology of carbon nanostructures in induced benzene transformation. *RSC Adv.* **2021**, *11*, 39428–39437. [[CrossRef](#)]
17. Lebedev, Y.A.; Krashevskaya, G.V.; Batukaev, T.S.; Mikhaylyuk, A.V. Time resolved study of ignition of microwave discharge in liquid hydrocarbons. *Plasma Process. Polym.* **2022**, *19*, e2100215. [[CrossRef](#)]
18. Bodrikov, I.V.; Kut'in, A.M.; Titov, E.Y.; Titov, D.Y.; Kurskii, Y.A.; Gazizullin, R.R. Fragmentation of thiophene and 3-methyl-2-thiophenecarboxaldehyde by direct liquid phase low-voltage discharges. *Plasma Process. Polym.* **2018**, *15*, 1800094. [[CrossRef](#)]
19. Shao, T.; Wang, R.; Zhang, C.; Yan, P. Atmospheric-pressure pulsed discharges and plasmas: Mechanism, characteristics and applications. *High Volt.* **2018**, *3*, 14–20. [[CrossRef](#)]
20. Rollier, J.D.; Gonzalez-Aguilar, J.; Petitpas, G.; Darmon, A.; Fulcheri, L.; Metkemeijer, R. Experimental study on gasoline reforming assisted by nonthermal arc discharge. *Energy Fuels* **2008**, *22*, 556–560. [[CrossRef](#)]
21. Eliasson, B.; Liu, C.J.; Kogelschatz, U. Direct conversion of methane and carbon dioxide to higher hydrocarbons using catalytic dielectric-barrier discharges with zeolites. *Ind. Eng. Chem. Res.* **2000**, *39*, 1221–1227. [[CrossRef](#)]
22. Li, M.W.; Tian, Y.L.; Xu, G.H. Characteristics of carbon dioxide reforming of methane via alternating current (AC) corona plasma reactions. *Energy Fuels* **2007**, *21*, 2335–2339. [[CrossRef](#)]

23. Matsui, Y.; Kawakami, S.; Takashima, K.; Katsura, S.; Mizuno, A. Liquid-phase fuel reforming at room temperature using nonthermal plasma. *Energy Fuels* **2005**, *19*, 1561–1565. [[CrossRef](#)]
24. Bilera, I.V.; Lebedev, Y.A. Plasma-Chemical Production of Acetylene from Hydrocarbons: History and Current Status (A Review). *Pet. Chem.* **2022**, *62*, 329–351. [[CrossRef](#)]
25. Wang, A.; Harrhy, J.H.; Meng, S.; He, P.; Liu, L.; Song, H. Nonthermal plasma-catalytic conversion of biogas to liquid chemicals with low coke formation. *Energy Convers. Manag.* **2019**, *191*, 93–101. [[CrossRef](#)]
26. Sarafraz, M.M.; Tran, N.N.; Pourali, N.; Rebrov, E.V.; Hessel, V. Thermodynamic potential of a novel plasma-assisted sustainable process for co-production of ammonia and hydrogen with liquid metals. *Energy Convers. Manag.* **2020**, *210*, 112709. [[CrossRef](#)]
27. Nomura, S.; Toyota, H.; Tawara, M.; Yamashita, H.; Matsumoto, K. Fuel gas production by microwave plasma in liquid. *Appl. Phys. Lett.* **2006**, *88*, 231502. [[CrossRef](#)]
28. Lin, L.; Zhou, W.; Gao, R.; Yao, S.; Zhang, X.; Xu, W.; Zheng, S.; Jiang, Z.; Yu, Q.; Li, Y.W.; et al. Low-temperature hydrogen production from water and methanol using Pt/ α -MoC catalysts. *Nature* **2017**, *544*, 80–83. [[CrossRef](#)]
29. Jahanmiri, A.; Rahimpour, M.R.; Shirazi, M.M.; Hooshmand, N.; Taghvaei, H. Naphtha cracking through a pulsed DBD plasma reactor: Effect of applied voltage, pulse repetition frequency and electrode material. *Chem. Eng. J.* **2012**, *191*, 416–425. [[CrossRef](#)]
30. Rusanov, V.D.; Babaritskii, A.I.; Baranov, I.E.; Bibikov, M.B.; Deminskii, M.A.; Demkin, S.A.; Zhivotov, V.K.; Konovalov, G.M.; Lysov, G.V.; Moskovskii, A.S.; et al. Nonequilibrium effect of atmospheric-pressure microwave-discharge plasma on methane and kerosene conversion into synthesis gas. *Dokl. Chem.* **2004**, *395*, 82–85. [[CrossRef](#)]
31. Wnukowski, M.; Moróń, W. Warm Plasma Application in Tar Conversion and Syngas Valorization: The Fate of Hydrogen Sulfide. *Energies* **2021**, *14*, 7383. [[CrossRef](#)]
32. Hartvigsen, J.; Elangovan, S.; Hollist, M.; Czernichowski, P.; Frost, L. Non-thermal plasma reformation of liquid fuels. *ECS Trans.* **2011**, *35*, 2825–2833. [[CrossRef](#)]
33. Babaeva, N.Y.; Tereshonok, D.V.; Naidis, G.V. Initiation of breakdown in bubbles immersed in liquids: Pre-existed charges versus bubble size. *J. Phys. D Appl. Phys.* **2015**, *48*, 355201. [[CrossRef](#)]
34. Han, R.; Li, C.; Wang, K.; Yuan, W.; Wang, Y.; Ding, W.; Ouyang, J. “Breakdown” of stratified electrical explosion products: Plasma development and its mechanical effect. *Phys. Fluids* **2021**, *33*, 107119. [[CrossRef](#)]
35. Liu, Y.; Dou, L.; Zhou, R.; Sun, H.; Fan, Z.; Zhang, C.; Ostrikov, K.K.; Shao, T. Liquid-phase methane bubble plasma discharge for heavy oil processing: Insights into free radicals-induced hydrogenation. *Energy Convers. Manag.* **2021**, *250*, 114896. [[CrossRef](#)]
36. Sharma, A.; Levko, D.; Raja, L.L.; Cha, M.S. Kinetics and dynamics of nanosecond streamer discharge in atmospheric-pressure gas bubble suspended in distilled water under saturated vapor pressure conditions. *J. Phys. D Appl. Phys.* **2016**, *49*, 395205. [[CrossRef](#)]
37. Titov, E.Y.; Titov, D.Y.; Bodrikov, I.V.; Kut’ın, A.M.; Kurskii, Y.A.; Gazizzulin, R.R. A device for generation of low-voltage discharges in liquid dielectric media. *High Energy Chem.* **2019**, *52*, 512–513. [[CrossRef](#)]
38. Sanchez-Minero, F.; Ancheyta, J.; Silva-Oliver, G.; Flores-Valle, S. Predicting SARA composition of crude oil by means of NMR. *Fuel* **2012**, *110*, 318–321. [[CrossRef](#)]
39. Fridman, A. *Plasma Chemistry*; Cambridge University Press: Cambridge, UK, 2008.
40. Cao, Y.B.; Zhang, L.L.; Xia, D.H. Catalytic aquathermolysis of Shengli heavy crude oil with an amphiphilic cobalt catalyst. *Pet. Sci.* **2016**, *13*, 463–475. [[CrossRef](#)]
41. Chen, M.; Li, C.; Li, G.-R.; Chen, Y.-L.; Zhou, C.G. In situ preparation of well-dispersed CuO nanocatalysts in heavy oil for catalytic aquathermolysis. *Pet. Sci.* **2019**, *16*, 439–446. [[CrossRef](#)]
42. Rakhmatullin, I.Z.; Efimov, S.V.; Tyurin, V.A.; Al-Muntaser, A.A.; Klimovitskii, A.E.; Varfolomeev, M.A.; Klochkov, V.V. Application of high resolution NMR (1H and 13C) and FTIR spectroscopy for characterization of light and heavy crude oils. *J. Pet. Sci. Eng.* **2018**, *168*, 256–262. [[CrossRef](#)]
43. Djimasbe, R.; Varfolomeev, M.A.; Al-Muntaser, A.A.; Yuan, C.; Feoktistov, D.A.; Suwaid, M.A.; Kirgizov, A.J.; Davletshin, R.R.; Zinnatullin, A.L.; Fatou, S.D.; et al. Oil dispersed nickel-based catalyst for catalytic upgrading of heavy oil using supercritical water. *Fuel* **2022**, *313*, 122702. [[CrossRef](#)]
44. Chesnokov, V.V.; Chichkan, A.S. Effect of catalysts on tar carbonization. *Catal. Today* **2021**, *379*, 28–35. [[CrossRef](#)]
45. Kozhevnikov, V.; Kozyrev, A.; Kokovin, A.; Semeniuk, N. The Electrodynamic Mechanism of Collisionless Multicomponent Plasma Expansion in Vacuum Discharges: From Estimates to Kinetic Theory. *Energies* **2021**, *14*, 7608. [[CrossRef](#)]
46. Abiev, R.S.; Sladkovskiy, D.A.; Semikin, K.V.; Murzin, D.Y.; Rebrov, E.V. Non-Thermal Plasma for Process and Energy Intensification in Dry Reforming of Methane. *Catalysts* **2020**, *10*, 1358. [[CrossRef](#)]
47. Khani, M.R.; Guy, E.D.; Gharibi, M.; Shahabi, S.S.; Khosravi, A.; Norouzi, A.A.; Shokri, B. The effects of microwave plasma torch on the cracking of Pyrolysis Fuel Oil feedstock. *Chem. Eng. J.* **2014**, *237*, 169–175. [[CrossRef](#)]
48. Zhang, S.; Gao, Y.; Sun, H.; Fan, Z.; Shao, T. Charge transfer in plasma assisted dry reforming of methane using a nanosecond pulsed packed-bed reactor discharge. *Plasma Sci. Technol.* **2021**, *23*, 064007. [[CrossRef](#)]
49. Hou, P.; Zhou, Y.; Guo, W.; Ren, P.; Guo, Q.; Xiang, H.; Li, Y.W.; Wen, X.D.; Yang, Y. Rational design of hydrogen donor solvents for direct coal liquefaction. *Energy Fuels* **2018**, *32*, 4715–4723. [[CrossRef](#)]
50. Chen, Q.; Yin, M.; Zhang, L.; Liu, H.; Qin, Z.; Wang, Z. Hydrogen-donated thermal upgrading of Venezuela extra-heavy oil: Identifying the role of hydrogen donor. *Pet. Sci. Technol.* **2020**, *38*, 550–555. [[CrossRef](#)]